Icarus **152**, 205–224 (2001)
doi:10.1006/icar.2001.6639, available online at http://www.idealibrary.com on IDEAL®

Making More Terrestrial Planets

J. E. Chambers

Armagh Observatory, Armagh, BT61 9DG, United Kingdom, and NASA/Ames Research Center, Mail Stop 245-3, Moffett Field, California 94035
E-mail: jec@star.arm.ac.uk

Received May 23, 2000; revised March 13, 2001; Posted online June 27, 2001

The results of 16 new 3D N-body simulations of the final stage of the formation of the terrestrial planets are presented. These N-body integrations begin with 150–160 lunar-to-Mars size planetary embryos, with semi-major axes $0.3 < a < 2.0$ AU, and include perturbations from Jupiter and Saturn. Two initial mass distributions are examined: approximately uniform masses, and a bimodal distribution with a few large and many small bodies. In most of the integrations, systems of three or four terrestrial planets form within about 200 million years. These planets have orbital separations similar to the terrestrial planets, and the largest body contains 1/3–2/3 of the surviving mass. The final planets typically have larger eccentricities, e, and inclinations, i than the time-averaged values for Earth and Venus. However, the values of e and i are lower than in earlier N-body integrations which started with fewer embryos. The spin axes of the planets have approximately random orientations, unlike the terrestrial planets, and the high degree of mass concentration in the region occupied by Earth and Venus is not reproduced in any of the simulations. The principal effect of using an initially bimodal mass distribution is to increase the final number of planets. Each simulation ends with an object that is an approximate analogue of Earth in terms of mass and heliocentric distance. These Earth analogues reach 50% (90%) of their final mass with a median time of 20 (50) million years, and they typically accrete some material from all portions of the disk.

Key Words: **accretion; planetary formation; Earth; terrestrial planets; extrasolar planets.**

1. INTRODUCTION

The Earth probably acquired many of its modern characteristics relatively late during its accretion. Our planet's mass, orbit, spin orientation, large satellite, and volatile inventory were probably determined some 10–100 Myr after the formation of the Solar System. These characteristics meant that Earth would provide a suitable environment for the origin and evolution of life. However, we currently know little about how and why our planet came to acquire its characteristics, and even less about whether it is typical or atypical of terrestrial planets in the Universe at large.

Current technology does not allow us to examine extrasolar Earth-sized planets, so we are limited to what we can glean from the cosmochemical record of the Solar System, observations of circumstellar disks, and computer models of planet formation. The evidence from these sources generally supports the "planetesimal hypothesis," in which the inner planets formed by accretion of a very large number of small bodies orbiting the young Sun in a disk (Safronov 1969; see Lissauer 1993, for a detailed review). Computer simulations have fleshed out this hypothesis. For example, simulations suggest that "runaway growth" took place early in the accretion process. Planetesimals in the disk with above average mass had large gravitationally enhanced collision cross sections, and accreted material faster than smaller bodies (Wetherill and Stewart 1989). Eventually, the largest objects swept up most of the solid mass in the disk and became "planetary embryos." Computer models of runaway growth suggest that it happened quickly (in less than 10^6 years in the inner Solar System), and predictably, different simulations produce broadly similar outcomes (e.g., Wetherill and Stewart 1993, Weidenschilling *et al.* 1997, Kokubo and Ida 1998, 2000).

The later stages of accretion happened much more slowly, and were highly stochastic. The planetary embryos collided with one another in giant impacts, and swept up the remaining planetesimals or scattered them onto unstable orbits, where they hit the Sun or were ejected from the Solar System. This process took at least 10^8 years, which is long compared to the formation times of Jupiter and Saturn. As a result, the final accretion of the inner planets occurred in the presence of perturbations from the giant planets.

Computer simulations of this final stage of accretion have succeeded in producing systems containing a handful of terrestrial planets between 0 and 2 AU from the Sun, moving on orbits that are very roughly circular and coplanar (e.g., Wetherill 1992, 1996, Chambers and Wetherill 1998, Agnor *et al.* 1999). However, these systems generally differ from the inner planets in several ways. The simulations consistently yield terrestrial planets with orbits that are more eccentric and inclined than those of Earth and Venus. Secondly, small planets such as, Mars and Mercury are rarely produced in the simulations. Objects with orbits similar to Mars or Mercury are almost always substantially more massive than either planet.

These difficulties imply that we have not yet reached the point where computer models tell us how terrestrial planets formed in

0019-1035/01 $35.00

detail. This is unfortunate because we would really like to use accurate models of planetary accretion in the Solar System to study the formation of Earth-like planets in other systems. Direct observation of these objects probably lies one or two decades in the future, but we can observe protoplanetary disks and giant planets orbiting other stars right now. The nature of these disks and giant planets are probably the two most important factors that determine the characteristics of extrasolar terrestrial planets (in addition to random chance). Once we truly understand the formation of the inner planets in the Solar System, we can combine these sources of information to deduce a great deal about extrasolar "Earths" even before they can be observed.

With this ultimate goal in mind, this paper presents 16 new N-body simulations of the final stage of accretion of the terrestrial planets. The aim is to build on the work of Chambers and Wetherill (1998; referred to as Paper I from now on) to begin assessing why the earlier simulations produced systems of terrestrial planets substantially different from the one we observe. In particular, we would like to know whether these differences occur because something important is missing in the models, or because our planetary system is atypical.

The new set of simulations differs from those of Paper I in several ways, with the changes introduced in the hope that they will lead to systems of terrestrial planets more like the Solar System. First, the simulations begin with more planetary embryos—about 150 per integration. Improvements in computer hardware and the integration algorithm make this possible, and it is desirable since it gives us better resolution of a problem which actually involved billions of bodies of various sizes.

The larger number of embryos makes it possible to investigate more realistic initial mass distributions. In particular, eight of the simulations presented here began with a bimodal mass distribution. Half of the mass was contained in a few large bodies with widely separated orbits, akin to the "oligarchic" embryos produced by the runaway growth simulations of Kokubo and Ida (1998). The remaining mass was divided amongst 10 times as many small bodies, designed to mimic the mass in residual planetesimals. The results of these simulations can be compared with the other eight, which began with more uniform mass distributions.

Two other changes are worth noting: the initial disk of embryos now has an inner edge at 0.3 AU, which in principle allows analogues of Mercury to form. And, unlike Paper I, the integration algorithm now retains spin information resulting from oblique collisions between embryos. The spin periods derived for the embryos in this way are probably unrealistically small, since loss of angular momentum in ejecta is not included in the integration algorithm. However, this method should provide some useful information about the post-accretion obliquities of the planets.

The initial conditions and integration procedure are described in more detail in Section 2. Next, Section 3 describes the results of the simulations, looking at the evolution in four sample cases, and examining the growth and orbital evolution of simulation objects that resemble Earth. In Section 4, the planetary systems produced by the simulations with the terrestrial planets are compared. The section includes a quantitative assessment of the similarities and differences by defining a set of statistics to describe any system of terrestrial planets. Finally, we will return to the question of whether differences are due to model shortcomings or the possibility that our planetary system is unusual.

2. SIMULATION DETAILS

This paper contains results from 16 N-body simulations, each beginning with 153–158 planetary embryos moving in three spatial dimensions. The embryos start in a disk with surface density $\sigma \sim \sigma_0(a/1\mathrm{AU})^{-3/2}$, where $\sigma_0 = 8\,\mathrm{g\,cm^{-2}}$. This surface density profile is similar to that for solids in a "minimum mass" solar nebula (Weidenschilling 1977). I also chose this steep surface density profile in the hope that it would help remedy the problem found in Paper I that Mars analogues were too massive. In the inner part of the disk, the initial surface density varies linearly from a maximum at 0.7 AU, to zero at 0.3 AU. This is designed to mimic the effects of mass loss resulting from fragmentation in the inner disk, where collision velocities are high (because of high Keplerian velocities). In addition, we hoped that this would produce analogues of Mercury with low masses.

The simulations are divided into batches of four. In the first batch (simulations 01–04), the embryos have a uniform initial mass of $0.0167M_\oplus$. In the second batch (simulations 11–14), the masses are proportional to σ, normalized to $0.0233M_\oplus$ at 1 AU. This dependency was chosen, since unlike Paper I, the initial embryos have masses that decrease with distance from the Sun (for $a > 0.7$ AU) rather than increasing in order to explore a new part of parameter space. In addition, it was hoped that using smaller embryos far from the Sun would help alleviate the "overweight Mars" problem alluded to earlier—smaller embryos will take longer to accrete, allowing more time for competing loss mechanisms to act.

The third and fourth batches of simulations started with bimodal mass distributions. Simulations 21–24 began with 14 large embryos of mass $0.0933M_\oplus$, and 140 smaller "planetesimals" of mass $0.00933M_\oplus$. The two types of bodies were each distributed in a disk, with each type contributing 50% of the total surface density at any location. Finally, the last batch of simulations (31–34) began with bimodal mass distributions, in which the masses of the embryos and the planetesimals were each proportional to the local surface density. These masses were normalized to $0.130M_\oplus$ and $0.0130M_\oplus$ at 1 AU, respectively.

In the first and second batches of simulations, the initial embryo spacings are small: about 4.2 Hill radii at 0.7 AU, where the disk density is highest, and about 2.4 Hill radii at the outer edge of the disk. This is similar to the spacing used in many previous simulations (e.g., Cox and Lewis 1980, Lecar and Aarseth 1986, Beauge and Aarseth 1990, Alexander and Agnor 1998). However, simulations of the formation of planetary embryos by Kokubo and Ida (1998) suggest that embryos typically form with

separations of ∼10 mutual Hill radii, equivalent to about 13 ordinary Hill radii. Such embryos are embedded in a sea of smaller bodies, whose total mass is of the same order of magnitude as the embryos themselves.

This result inspired the choice of initial conditions for the third and fourth batches of integrations in this paper, which used bimodal mass distributions. In these cases, the initial spacings of the larger "runaway" embryos were about 26 Hill radii at 0.7 AU, and about 15 Hill radii at the outer edge of the disk. Thus, the first and second batches on the one hand, and the third and fourth batches on the other, should bracket the range of likely outcomes of the runaway growth stage.

The initial eccentricities and inclinations for these simulations were chosen randomly in the range $0 < e < e_0$ and $0 < i < i_0$. In simulations 01, 02, 11, 12, 21, 22, 31, and 32, $e_0 = 0.01$ and $i_0 = 0.5^\circ$, while in the other 8 simulations $e_0 = 0.1$ and $i_0 = 5^\circ$. The initial arguments of perihelion, nodal longitudes, and mean anomalies where chosen at random.

Jupiter and Saturn were included in each integration from the beginning. The giant planets started with their current orbits and masses, and interacted fully with the embryos and planetesimals. In addition, the initial orbits of Jupiter and Saturn were rotated so that the disk of embryos lay in the invariable plane of the Jupiter–Saturn system.

Collisions between objects were assumed to be totally inelastic, so that each collision conserved mass and linear momentum, and produced a single new body. The new object retained any excess angular momentum resulting from an oblique impact as spin angular momentum. In principle, this allows us to calculate the spin rate and obliquity of any object that has accreted another body. Collisions were determined by assuming that the embryos are spherical, with radii corresponding to a material density of 3 g cm^{-3}.

The integrations used a new hybrid symplectic integrator algorithm (Chambers 1999) and the *Mercury* integrator package (Chambers and Migliorini 1997). The integration algorithm is a substantial improvement over the combination of symplectic and nonsymplectic integrators used in Paper I. The typical energy error at the end of one of these integrations (excluding energy loss because of collisions) was about 1 part in 10^4. The hybrid integrator parameters are a stepsize of 7 days, and a Bulirsch–Stoer tolerance of 10^{-11}.

In order to avoid excessive integration errors (which rise rapidly with decreasing heliocentric distance r for a fixed-timestep integrator) bodies were assumed to collide with the Sun if their heliocentric distance fell below 0.1 AU. It might be thought that this approximation would artificially bias the results of the integrations by prematurely removing material on eccentric orbits or orbits with small semi-major axes. In practice, these effects turned out to be minor. For example, in simulations 01 and 21, 65 objects were removed with $r < 0.1$ AU. Of these, 55 had $a > 1.8$ AU just prior to their removal. These objects were in, or close to, the asteroid belt, clustered around the ν_6 and 3 : 1 mean-motion resonances. Such objects are likely to have short lifetimes before they would truly hit the Sun. Objects with initially circular orbits in the ν_6 and 3 : 1 resonances have lifetimes ∼1 million years (Gladman *et al.* 1997), and these lifetimes will be substantially shorter for bodies on highly eccentric orbits. Because of their high eccentricities, these objects have very high velocities with respect to other embryos. As a result, they interact only weakly during close encounters, and gravitational focusing is essentially absent, so their collision probabilities are very low. Only one of the 65 bodies removed with $r < 0.1$ AU had $a < 1$ AU, which suggests that this approximation will not significantly affect the amount of material available for accretion onto Mercury analogues. In summary, most of the material removed with $r < 0.1$ AU is likely to have hit the Sun soon afterward without significantly interacting with other embryos in the meantime.

3. RESULTS

3.1. Sample Evolutions

Figures 1–4 show the evolution of four of the simulations, one from each batch. Each symbol in the figures shows the semi-major axis, a, and eccentricity, e, of an embryo, where the radius of the symbol is proportional to the radius of the embryo. Note that the values of e and a are the instantaneous values. The embryos' eccentricities generally undergo large oscillations on timescales of 10^4–10^6 years (see Paper I).

Figure 1 shows the evolution of simulation 03, which began with 153 equal mass embryos with eccentricities $0 < e < 0.1$ and inclinations $0 < i < 5^\circ$. These values of e and i are quite large, so gravitational focusing during close encounters was weak. As a result, the collision rate was low, even at the beginning of the integration. For example, only three collisions occurred during the first 100,000 years of the integration. In simulation 01, in which e and i were initially smaller by a factor of ten, 24 collisions occurred in the same amount of time.

In simulation 03, the orbits became more dynamically excited with time. Near the outer edge of the disk, e increased rapidly as a result of strong secular perturbations from the giant planets, which peak at the ν_6 resonance at 2.1 AU. Objects in the ν_6 resonance experience large, chaotic oscillations in e. These oscillations are driven by the coincidence of the rate of precession of the orbit's longitude of perihelion with an eigenfrequency of the planetary system (which roughly corresponds to the precession frequency of Saturn's longitude of perihelion). As the simulation continued, this excitation propagated to other parts of the disk, as embryos with large e were scattered to smaller a via close encounters. Some of the embryos were excited to sufficiently large values of e that they fell into the Sun. In simulation 03, about 25% of the initial mass was lost, almost all of it colliding with the Sun. The corresponding figures for the other simulations are comparable, although somewhat lower for the simulations with initially bimodal mass distributions. The mean mass losses for simulations 01–14 and 21–34 were 27% and 22%, respectively.

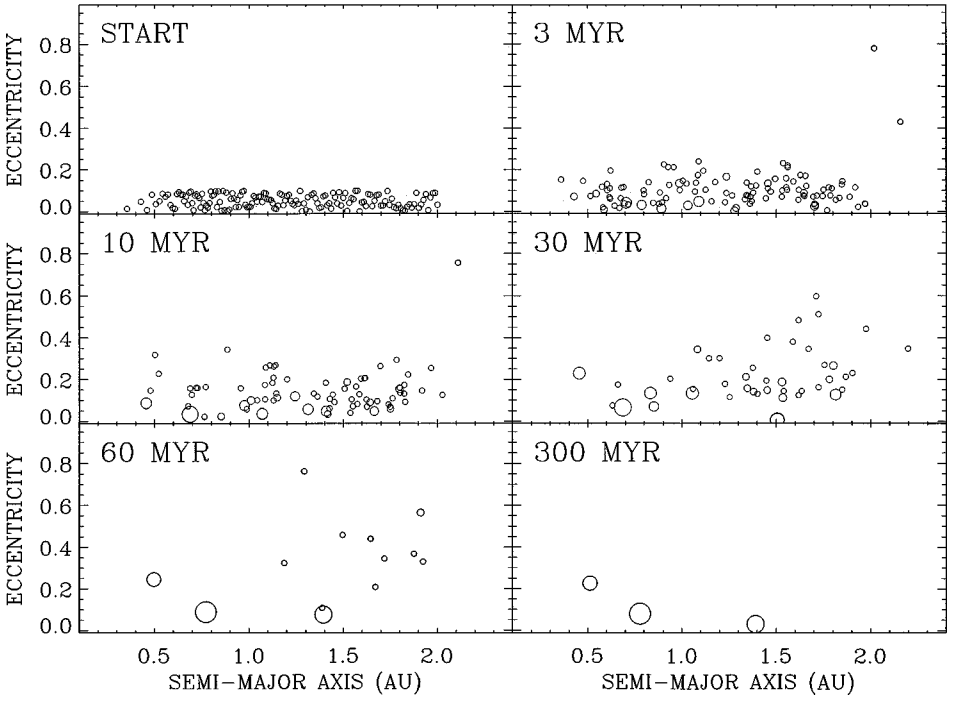

FIG. 1. Evolution of the semi-major axes and eccentricities of embryos from simulation 03. The symbol radius is proportional to the radius of an embryo.

In simulation 03, accretion occurred most rapidly in the inner part of the disk, and the largest objects in this region grew to $\sim 0.2 M_\oplus$ within a few million years. The accretion rate then slowed considerably. By ∼60 million years, all the material in the inner part of the disk had been accreted by two objects, the larger of which had a mass similar to Earth with an orbit similar to Venus. A third large object with a mass of about $0.5 M_\oplus$ lay further from the Sun with an orbit similar to that of Mars.

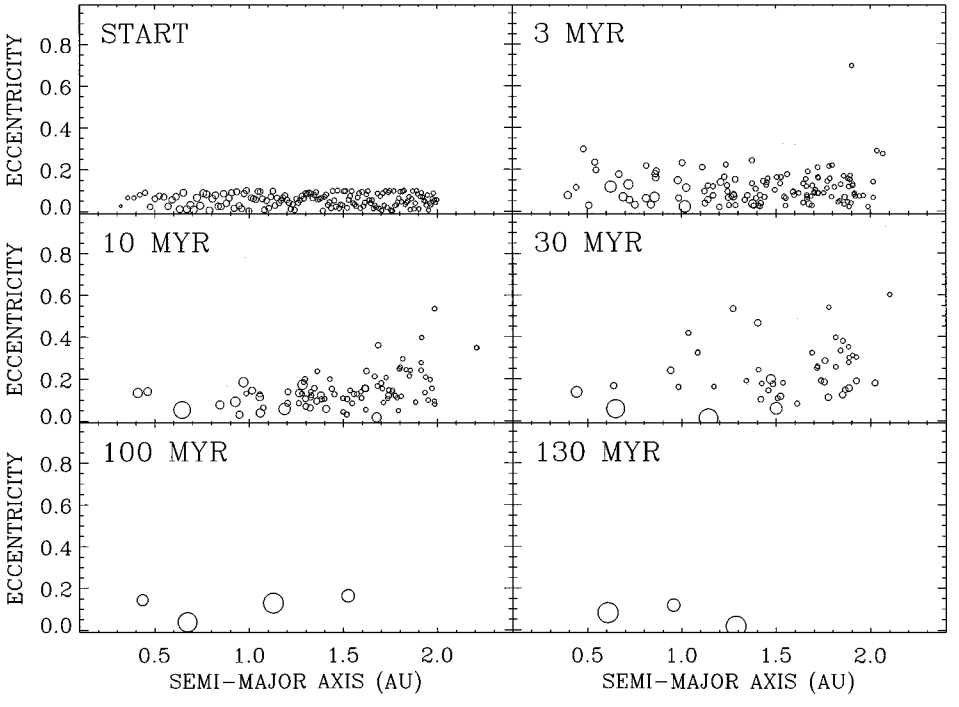

FIG. 2. Evolution of the semi-major axes and eccentricities of embryos from simulation 13. The symbol radius is proportional to the radius of an embryo.

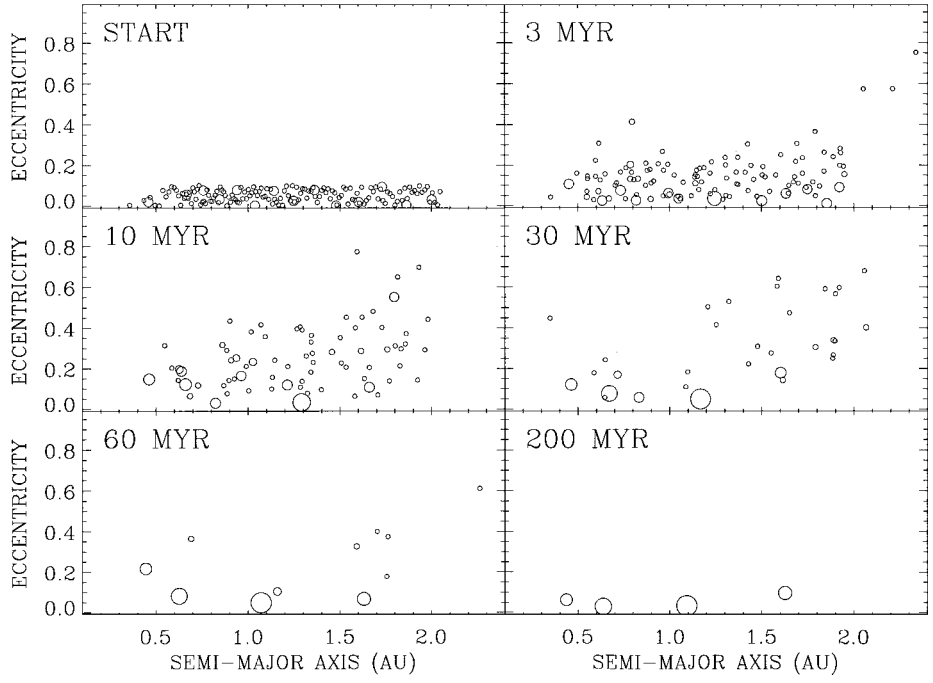

FIG. 3. Evolution of the semi-major axes and eccentricities of embryos from simulation 23. The symbol radius is proportional to the radius of an embryo.

However, this outer region still contained about 10 other bodies, mainly embryos which had undergone no accretion since the start of the simulation. Over the remainder of the integration, these objects were accreted by the larger bodies or fell into the Sun in roughly equal numbers, leaving only the three large bodies remaining. The orbits of these large bodies experienced only minor changes from 60 million years onward.

Figure 2 shows the evolution of simulation 13, which began with 158 embryos with initial masses that increased rapidly with distance from the Sun up to a maximum at $a = 0.7$ AU, and

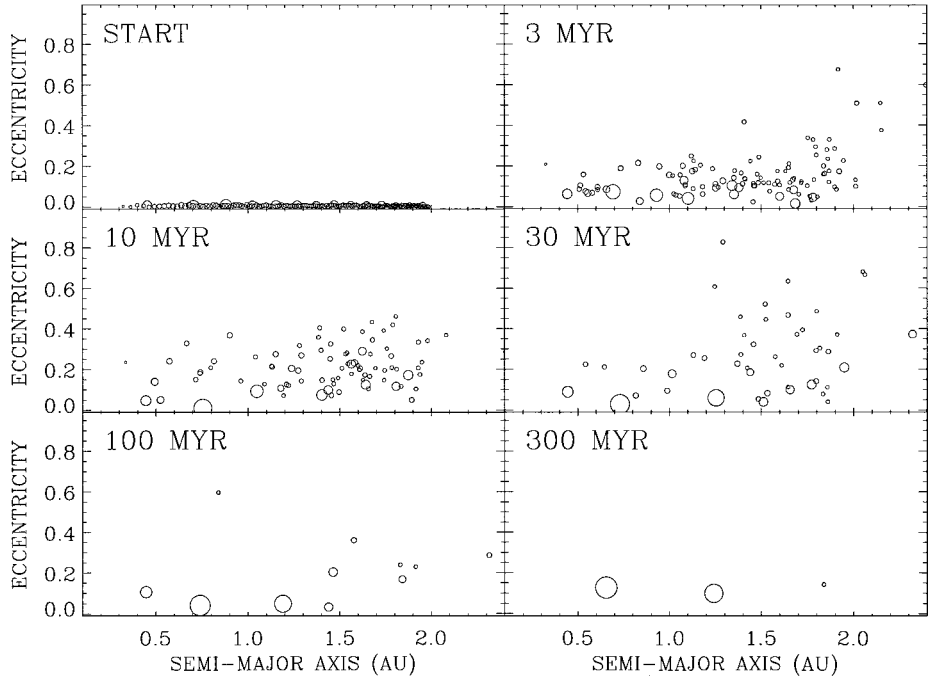

FIG. 4. Evolution of the semi-major axes and eccentricities of embryos from simulation 32. The symbol radius is proportional to the radius of an embryo.

then decreased with distance after that. The early stages of the evolution were similar to that in Fig. 1. Accretion was most rapid in the inner part of the disk, and strong orbital excitation occurred near $a = 2$ AU, which gradually propagated to smaller a. The early accretion rate was also similar to simulation 03. However, one object grew faster than the others, and by 10 million years a "proto-Venus" of about half an Earth mass had formed at $a \sim 0.6$ AU. This planet subsequently grew more slowly, while a second larger body accreted at $a \sim 1.1$ AU.

By 30 million years, 63% of the original mass was contained in four large objects, and these had orbits and masses quite similar to the terrestrial planets. The remaining mass existed in about 40 smaller planetary embryos, most having $a > 1$ AU. The four large bodies swept up or scattered all the other embryos by 100 million years, and formed what appeared to be a stable system. However, the outer two bodies ("Earth" and "Mars") were too close together—their orbital eccentricities meant that their orbits almost crossed one another. Eventually they had a close encounter which caused them to swap places. This brought Mars into close proximity with "Venus," which perturbed Venus's orbit enough to cause it to cross the orbit of "Mercury." The end result was that the inner two planets collided with one another, and the outer two planets swapped places. The final system contained three planets in an unusual configuration: two large bodies and a smaller one in between.

Figure 3 shows simulation 23, which began with 154 embryos with a bimodal mass distribution. Half the initial mass was contained in 14 large embryos, and half in 140 smaller "planetesimals." The wide range of masses meant that partial equipartition of random orbital energy ("dynamical friction") occurred, and for most of the integration the large embryos had lower e and i than most of the small planetesimals, as can be seen in Fig. 3. Early in the integration, the orbital excitation of the small planetesimals was larger than that of small bodies in simulations 03 and 13, while the excitation of the large embryos in simulation 23 was comparable to that of the largest bodies in the earlier integrations. This apparently contradictory behavior presumably occurs because the largest bodies in simulation 23 are somewhat more massive than the largest bodies in simulations 03 and 13 at early epochs, which partially offsets the greater dynamical friction in the former case, while the small bodies are less massive than those in simulations 03 and 13.

In simulation 23, the mass difference between the embryos and planetesimals was large enough that the embryos did almost all of the accreting. A few planetesimals collided with and accreted other planetesimals, but never gained enough mass to close the gap with the embryos. At 10 million years, the largest embryo had a mass of about $0.6 M_\oplus$ and $a \sim 1.3$ AU. This object had accreted four other embryos so far, plus a small amount of mass in planetesimals. Unlike Figs. 1 and 2, in this simulation a "protoEarth" formed before a proto-Venus.

By 30 million years, only five embryos remained. About 25 planetesimals were still present, most of which had undergone no accretion. Subsequently, two of the embryos collided, the residual planetesimals were swept up or fell into the Sun, and a system of four planets formed, with characteristics quite similar to the terrestrial planets. This system proved to be more stable than that of Fig. 2 at 100 Ma, and no further collisions took place. In this simulation, the structure of the final system of planets was determined at an early stage—most of the final characteristics were apparent at 30 million years, and accretion was almost complete by 60 million years.

Figure 4 shows simulation 32, which began with 14 large embryos and 140 smaller planetesimals. The masses of both the embryos and the planetesimals were a function of semi-major axis in a way analogous to the objects in simulation 13 (see Fig. 2). However, at any point in the disk the embryos were 10 times as massive as the planetesimals. In this integration, the initial values of e and i were low, leading to quite rapid collisional evolution at first (eight collisions occurred in the first 10^5 years). However, the mean e and i increased rapidly, and were soon comparable to values for simulations beginning with larger e and i.

Partial equipartition of random orbital energy was apparent as in simulation 23. The large embryos typically had smaller e and i than the less massive planetesimals. Dynamical excitation was also pronounced near the ν_6 secular resonance, and both embryos and planetesimals were vulnerable to being lost as a result (e.g., the embryo at $a = 2.3$ AU in the 30 million year panel of Fig. 4 is about to be lost).

The situation at 30 and 100 million years was broadly similar to Fig. 3. In each case there were three large planets with $a < 2$ AU, and a number of bodies further from the Sun. However, in the simulation of Fig. 4, the inner two planets lay close to a secular resonance with one another, in which their perihelia precessed at the same rate. As the two planets moved in and out of this resonance, their eccentricities increased until their orbits become crossing, and they collided. Meanwhile, most of the planetesimals in the outer part of the disk were removed, leaving one tiny survivor with about half the mass of the Moon, moving on an apparently stable orbit just inside the asteroid belt.

3.2. Orbital Excitation

One of the problems identified with the simulations in Paper I was that the final planets had large orbital eccentricities and inclinations. In Figs. 1–4 is it clear that e becomes large for many of the embryos in the new simulations, although dynamical friction means that the most massive bodies tend to have more nearly circular orbits.

Figure 5 shows the mass-weighted mean eccentricity, $\bar{e}$, versus time in four of the new simulations. Note the change in the scale of the x axis at 1 million years. In simulations 03, 13, and 23, which began with large initial e, the mass-weighted eccentricity rose rapidly during the first few hundred thousand years because of close encounters and secular interactions between embryos.

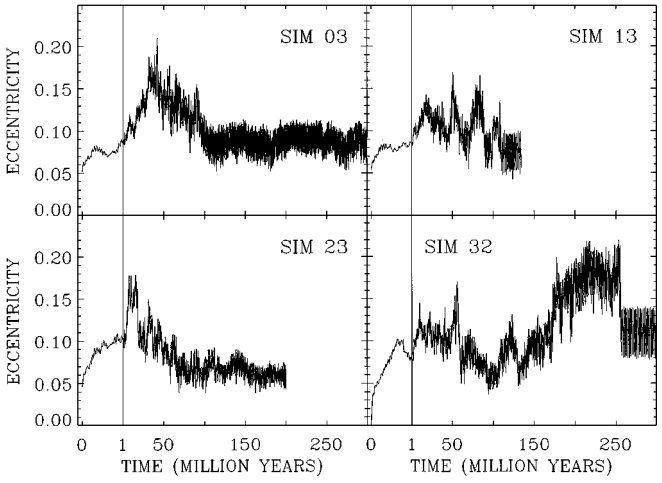

FIG. 5. Mass-weighted eccentricity versus time for the simulations shown in Figs. 1–4. Note the change in scale of the x-axis at 1 million years.

In simulation 32, which began with initial values of e between 0 and 0.01, the initial rise was greater, but after 0.5 million years, $\bar{e}$ had become similar to the other simulations. This time is comparable to the timescale for planetary embryos to form, which suggests that embryos probably had $e > 0.01$ at the end of the runaway growth stage of accretion.

The rate of increase in $\bar{e}$ slows dramatically in each simulation when $\bar{e}$ reaches about 0.1. At this stage, the largest embryos contain 0.1–0.2 Earth masses, and have escape velocities of 5 to 6 kms^{-1}. At $a = 1$ AU, this corresponds to about 20% of the orbital velocity. After a few close encounters with such bodies, a typical embryo/planetesimal would have an eccentricity of up to 0.2.

At later times the behavior of $\bar{e}$ varies from one simulation to another, but generally $\bar{e}$ rises to a maximum of 0.15–0.2 at 50–100 million years, and then declines slightly. This decline has two causes. First, collisions between embryos on eccentric orbits tend to produce a new body moving on a more circular orbit. Second, embryos with very high eccentricities are ultimately removed by collisions with the Sun or ejection from the Solar System. This "dynamical evaporation" is somewhat analogous to cooling of a liquid by escape of the most energetic molecules from its surface.

In the late stages of simulation 32, a deviation from this trend is apparent. In this integration, $\bar{e}$ increased after about 150 million years. This was primarily due to a near secular resonance between two of the largest embryos. These objects ultimately collided, reducing $\bar{e}$, but leaving a system that was still somewhat more excited than average.

Another way to assess the degree of orbital excitation is to use the angular momentum deficit (Laskar 1997). This measures the difference between an orbit's z-component of angular momentum, and that for an orbit with the same semi-major axis having zero e and i. Figure 6 shows the normalized angular momentum deficit (S_d) for the simulations shown in Fig. 5, where S_d is given by

$$S_d = \frac{\Sigma_j m_j \sqrt{a_j}\left[1 - \sqrt{\left(1 - e_j^2\right)}\cos i_j\right]}{\Sigma_j m_j \sqrt{a_j}}. \qquad (1)$$

The behavior in Fig. 6 is somewhat different than in Fig. 5. Although both $\bar{e}$ and S_d are mass weighted, the former depends mostly on e of the largest bodies whereas the latter is strongly influenced by e and i of the smaller bodies also. This is because dynamical friction tends to give low-mass bodies large eccentricities and inclinations, and orbits with large e and i make large contributions to S_d (it is proportional to $e^2 + i^2$ for small e and i). This is apparent in the occasional spikes seen in Fig. 6, which are each due to a single body moving on a highly eccentric orbit. These bodies quickly fall into the Sun, at which point S_d is reduced again.

Because single objects can make large contributions to S_d, its behavior is less smooth than $\bar{e}$ as long as orbital and accretional evolution is still taking place. This allows us to pinpoint the damping effects of individual collisions and "evaporations," which is difficult using $\bar{e}$. For example, the large drop in S_d at 0.8 Myr in simulation 32 is caused when the outermost large embryo falls into the Sun. Correlating changes in S_d with collisions or removal events suggest that the loss of high-e objects when they hit the Sun plays a larger role than collisions between embryos in damping the orbital excitation of the whole system. However, both processes play a part.

When accretion ceases, $\bar{e}$ still undergoes large oscillations. Conversely, S_d is generally quite well conserved, except in cases such as simulation 01, in which there is strong coupling between the terrestrial planets and Jupiter and Saturn (in this simulation, one final planet is in the ν_5 secular resonance). S_d usually falls significantly when accretion ceases and the last planet-crossing

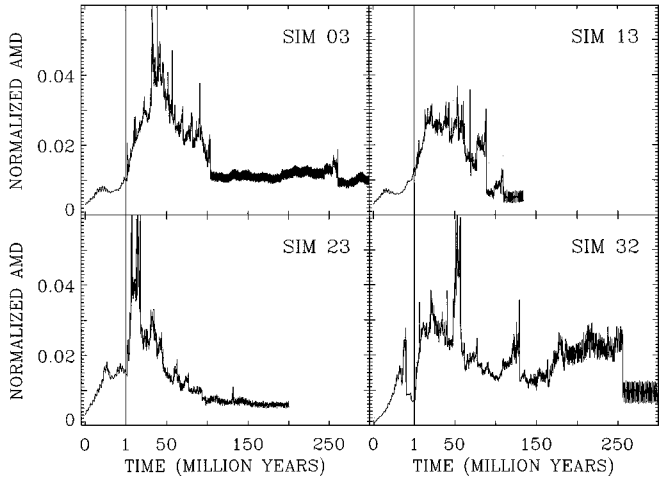

FIG. 6. Normalized angular momentum deficit versus time for the simulations shown in Figs. 1–4. Note the change of scale of the x-axis at 1 million years.

body is removed. At this point, S_d generally has a value similar to that during the first million years of the integration. However, $\bar{e}$ usually undergoes a much smaller change upon completion of accretion. This suggests that the time-averaged eccentricities of the largest bodies (which dominate the contributions to $\bar{e}$) do not change significantly once these bodies have formed.

3.3. Evolution of Earth Analogues

In most of the 16 simulations, it is possible to identify objects at the end of the integration which are reasonable analogues of Earth and Venus in terms of mass and semi-major axis. (This is usually not true for Mercury and Mars.) We can use these analogues to gauge possible dynamical and accretional histories for Earth and Venus. In systems containing two final planets, the inner object "Venus" and the outer object "Earth" are designated. When $N = 4$, the second and third planets were chosen to be Venus and Earth. For cases with $N = 3$, the choice is somewhat subjective; in general, the inner and outer of the two largest planets are chosen to be Venus and Earth, respectively.

Figure 7 shows the mass of Earth analogues versus time in 4 simulations. In simulations 01–14, objects destined to become Earth analogues usually undergo rapid accretion during the first few million years, typically reaching about 20% of their final mass by this time. The accretion rate then slows down. In simulations 21–34, which began with some large embryos, this phase of accretion is less pronounced.

At later times, Earth analogues typically go through two more growth phases, with mass growing approximately linearly with time in each phase. This is clearly apparent in simulation 13 in Fig. 7, where there is a rapid rise in mass until about 30 million years, followed by slower accretion at later times. The first of these latter phases appears to be associated with the formation of a few large protoplanets in the inner parts of the disk, while the second phase is characterized by accretion of residual smaller bodies, mostly from the outer part of the disk. In a few cases, however, (e.g., simulation 03) the latter phase is absent.

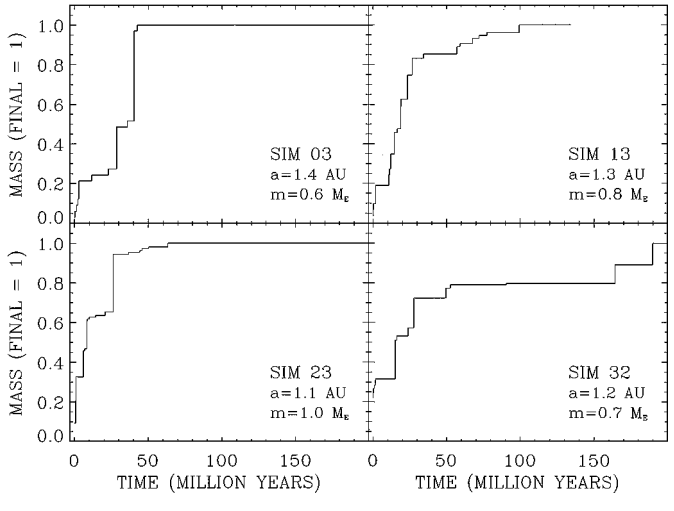

FIG. 7. Mass versus time for Earth analogues in the simulations shown in Figs. 1–4.

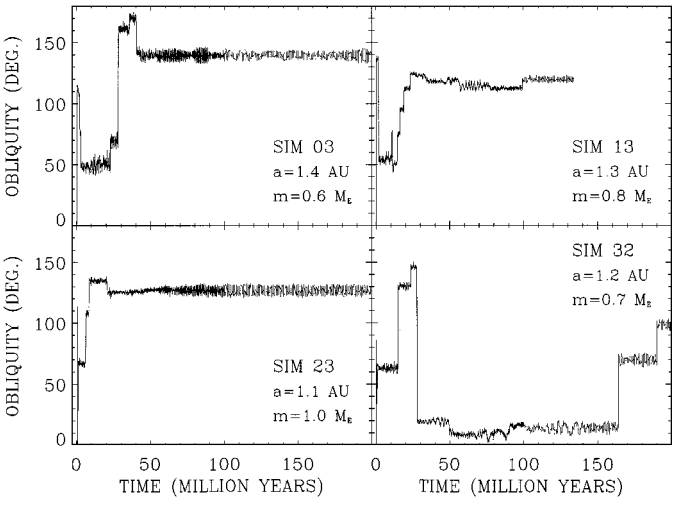

FIG. 8. Obliquity versus time for Earth analogues in the simulations shown in Figs. 1–4.

The median times required for Earth analogues to reach 50% and 90% of their final mass are 20 and 54 Myr, respectively, for the 16 simulations. The median times are similar for the simulations using uniform initial masses and those starting with bimodal mass distributions (22, 19 Myr for 50% final mass, and 53, 56 Myr for 90%, respectively) despite the larger initial masses of embryos in the bimodal mass cases.

Most of the Earth analogues experienced giant impacts during their formation. For example, the Earth analogue in simulation 03 was hit by another body of almost equal mass at about 40 million years, and this impact was essentially the last accretion event. In other cases, such as the Earth analogue in simulation 13, the largest impactor contributed only about 10% of the final mass. This diversity illustrates the stochastic nature of accretion in these simulations. However, the range of behaviors is consistent with the finding of Agnor *et al.* (1999) that the Earth could have been hit by an impactor with mass greater than that of Mars, 50–100 million years after the formation of the Solar System, which led to the formation of the Moon.

The most massive impactor to hit the Earth analogues in each of the simulations has a median mass of $0.22 M_\oplus$. For these collisions, the impactor has a median mass of 0.67 times that of the target. In other words, most Earth analogues were hit by another body of comparable size at some point in their accretion.

Figure 8 shows the obliquity evolution of the 16 Earth analogues. The high frequency oscillations in the figure are caused by small variations in the orbital inclinations. The abrupt jumps are due to collisions with other bodies. These collisions are usually oblique, so they reorient the spin axis of the body. In some cases, this can cause very large changes in the spin orientation. For example, the Earth analogue in simulation 03 changed from

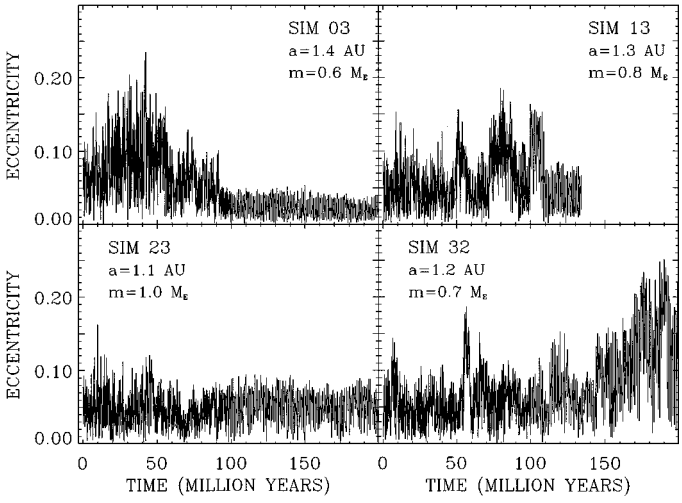

FIG. 9. Eccentricity versus time for Earth analogues in the simulations shown in Figs. 1–4.

a prograde rotation with obliquity of about 70° to a retrograde rotation with an obliquity of about 160° in a single impact at about 30 million years.

In most of the simulations, the approximate final obliquity was determined during the first 50 million years or so, since this was when the Earth analogues experienced most giant impacts. However, in three of simulations 31–34, the Earth analogues experienced substantial spin axis reorientations at much later times. An extreme example is simulation 32, which was transformed from a prograde rotator with obliquity comparable to Earth, to a retrograde rotator spinning almost on its side. This transition was caused by two relatively modest impacts, with bodies each about 10% of the final mass of the planet, occurring later than 150 Myr.

Figure 9 shows the eccentricity evolution for the Earth analogues of Figs. 7 and 8. The high-frequency oscillations in e with amplitude $\sim$0.1 are caused by secular perturbations by neighboring planetary embryos and the giant planets. This is similar to the behavior found in Paper I. These secular oscillations are large enough that changes in e caused by impacts do not stand out. A few of the features in Fig. 9 are correlated with changes in the mass-weighted mean eccentricity, $\bar{e}$, and normalized angular momentum deficit seen in Fig. 5 and 6. For example, this is true for the early excitation and subsequent damping in simulation 03, and the late excitation in simulation 32. However, the e of the Earth analogues does not always follow the system as a whole. For example, the eccentricity of the Earth-like planet in simulation 23 undergoes oscillations of roughly constant amplitude despite large changes in $\bar{e}$ and S_d.

For the 16 simulations presented here, there is no overall tendency for e of Earth analogues to increase or decrease in the late stages of the integrations. In roughly one quarter of the simulations, e decreases in the late stages of accretion, usually because of changes in the secular perturbations by other large bodies. However, in another quarter of the simulations, e is excited in the final stages of accretion. This is true in simulation 32, in which two of the embryos enter a near secular resonance with one another, which also excites the eccentricities of other bodies in the system. In the remaining 50% of the simulations (e.g., simulations 13 and 23 in Fig. 9), the eccentricity of Earth analogues is established early in the integration. In these cases there is no substantial late-stage excitation or damping in e.

The evolution of Venus analogues is similar to that of Earth analogues. At early times, the former grew slightly faster than the latter, reaching 50% of their final mass in a median time of 15 Myr. At later times, the accretion slowed down, and the Venus analogues reached 90% of their final mass in a median time of 62 Myr. There is a considerable spread in this later time. In one extreme case (Simulation 32), "Venus" reached 90% of its final mass 255 Myr after the start of the integration. Conversely, in some simulations Venus was 90% complete after 30–40 Myr. There is a weak correlation between the 50% formation times of Earth and Venus analogues, and also for the 90% formation times. However, the 50% and 90% formation times for the same planet appear to be uncorrelated. Hence, the Earth and Venus analogues tended to grow at similar rates to one another, but the early accretion rate was not a good indicator of the later accretion rate.

3.4. Final Systems

Figure 10 shows the final configurations of the 16 simulations. Each row of symbols in the figure shows the results of one simulation, with symbols representing planets. The radius of a symbol is proportional to the radius of the planet. The horizontal lines through each symbol indicate the perihelion and aphelion distances of the planet's orbit, and the arrows show the

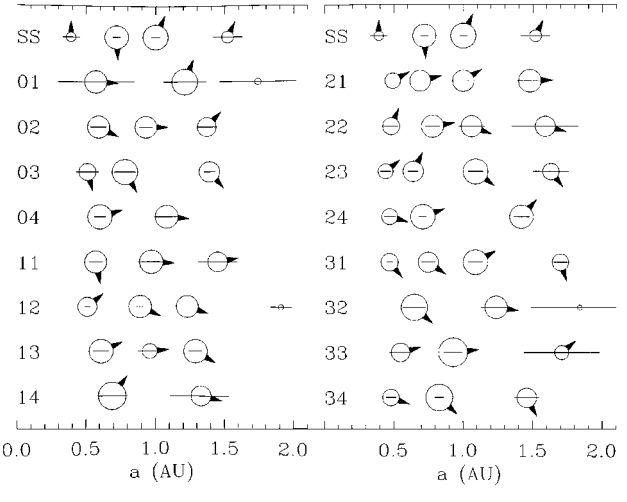

FIG. 10. Final states of the 16 simulations, where "SS" refers to the inner planets of the Solar System, and "01" refers to simulation 01, etc. Each circle represents a planet with radius proportional to the radius of the symbol. Horizontal lines indicates perihelion and aphelion distances, and arrows indicate the orientations of the planets' spin axes.

orientation of the planet's spin axis with respect to its orbital plane (upward-pointing arrows imply obliquities $<90^\circ$, while down arrows imply obliquities $>90^\circ$.)

Systems with three or four terrestrial planets are common, while in two cases only two planets formed. The simulations presented in this paper typically produced more final planets than the simulations of Paper I, which often ended with only two planets. The final planets in the new simulations have widely spaced orbits when measured in Hill radii, and moderate eccentricities and inclinations. The obliquities ϵ are such that $\cos\epsilon$ is distributed approximately at random.

Simulations 21–34, which began with bimodal mass distributions, tended to produce more planets (3.5 ± 0.5) than simulations 01–14 (2.9 ± 0.6), which began with more uniform mass distributions. Within each set of integrations the results are quite similar in terms of the number of planets, their masses, and semi-major axes. This is in contrast to Paper I, where the results varied greatly from one simulation to the next, even when the initial conditions were similar. Simulations that began with small values of e and i show some tendency to end with more planets (3.4 on average) compared to integrations with large initial e and i (2.9 on average).

Figure 11 shows the distribution of masses, m, as a function of semi-major axis for all the final planets in the simulations. The figure also shows the results of Model B from Paper I for comparison. (Of the three models presented in Paper I, Model B had initial conditions that most closely resemble those used in this paper.) The square symbols in each figure represent the terrestrial planets of the Solar System. The planetary systems described in Paper I had an m–a distribution quite different from the terrestrial planets. In those simulations, the planetary masses tended to decrease with distance from the Sun, rather than increasing at first, peaking in the middle and then decreasing, as they do in the Solar System.

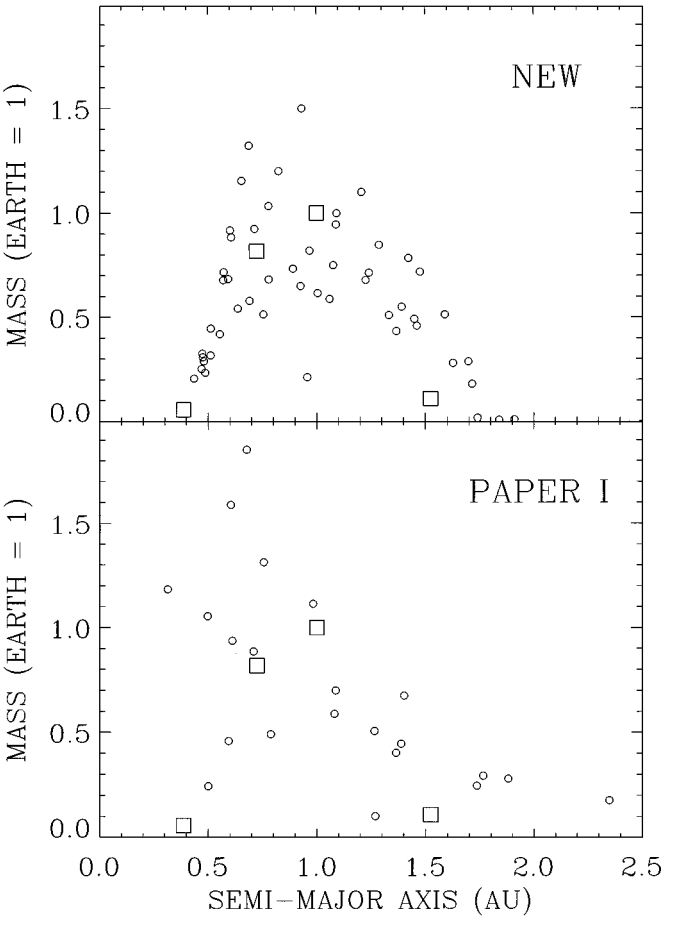

FIG. 11. Mass versus semi-major axis for planets produced by the simulations reported here and those of Model B from Paper I.

The simulations described in this paper have an m–a distribution that resembles that of the terrestrial planets. The most massive objects have $0.6 < a < 1.2$ AU, and objects outside this range tend to be smaller. The least massive planets usually have $a < 0.5$ AU or $a > 1.5$ AU. However, planets with orbits similar to Mars and Mercury generally are more massive than these planets. Wetherill (1992, 1996) obtained rather similar results in simulations using the Öpik–Arnold method, although Wetherill (1992) also found many cases of low-mass planets in the region occupied by Earth and Venus in the Solar System.

The analogues of Mercury are large despite the fact that the initial surface density profile was chosen to keep the amount of mass in the innermost part of the disk quite low. Simulations 11–14 and 31–34, in which the embryos decreased in size with distance from the Sun, often produced Mars analogues that are more massive than this planet, just like the other simulations presented here and the simulations in Paper I. Interestingly, three of the new simulations ended with very small objects on orbits with $1.5 < a < 2.0$ AU. These bodies are all approximately lunar-mass embryos that underwent no collisions during the integration. This provides some encouragement that the small mass of the real Mars can be explained, but note that these low-mass objects all had orbits further from the Sun than Mars does.

The largest planet in each system has a mass similar to Earth. This reflects the fact that the simulations began with total mass $\sim 2.5 M_\oplus$, and typically ended with two or three large planets. All of the final planets have $0.3 < a < 2.0$ AU, corresponding to the initial extent of the disk of embryos. Several bodies in each simulation entered the inner asteroid belt, but they were subsequently either lost or returned to the terrestrial-planet region.

Figure 12 shows the eccentricity versus mass distribution for the final planets in the systems described here, and those of Paper I. The eccentricities, e, have been time-averaged in each case. The values of e are generally somewhat smaller in the new integrations than in the old, with the lowest values comparable to the time-averaged values for Earth and Venus. The median value in the simulations, $e = 0.08$, is somewhat larger than for Earth and Venus, but comparable to the time-averaged eccentricity of

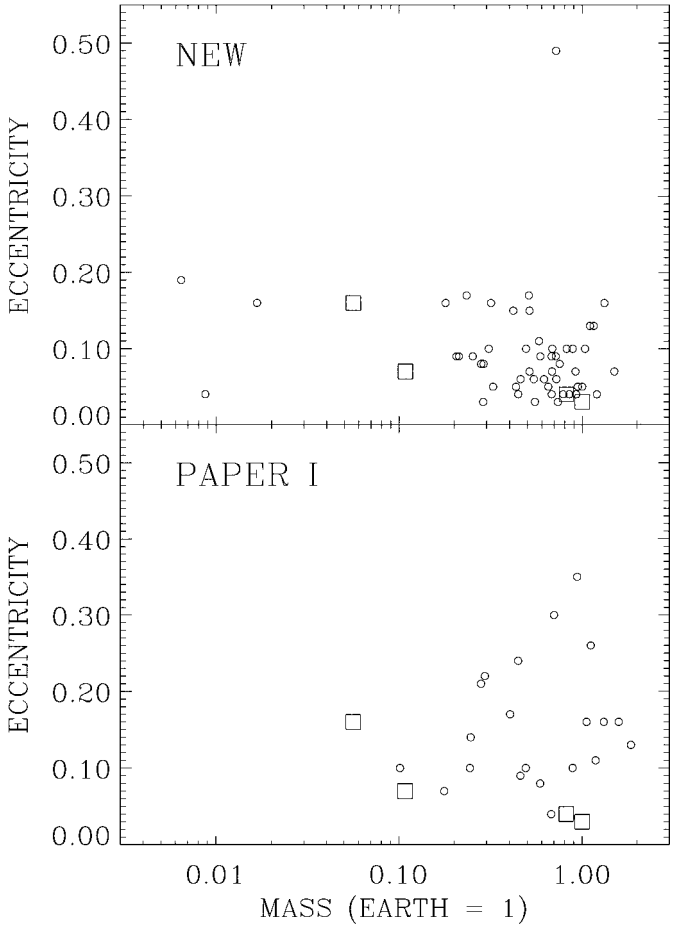

FIG. 12. Eccentricity versus mass for planets produced by the simulations reported here and those of Model B from Paper I.

Mars. In contrast to the terrestrial planets, there is apparently no correlation between e and m in Fig. 12.

Figure 13 shows the composition of the final planets in terms of their constituent embryos. The embryos are color-coded in terms of their initial semi-major axes, with four different shades of grey implying zones bounded by 0.7, 1.1, and 1.5 AU. The radius of each pie-chart symbol is proportional to the radius of the planet.

The figure indicates that a considerable amount of radial mixing of material occurred during the simulations. However, the final planets have a composition gradient which preserves some memory of the initial distribution of embryos (this is similar to the result found by Wetherill (1994)). The planets are predominantly composed of embryos from one or two zones closest to their final semi-major axis. This is especially true of small planets that are closest to or furthest from the Sun (possible analogues of Mercury and Mars). In particular, the "Mercuries" tend to contain material that mostly comes from the innermost zone, while "Marses" are mostly made of embryos from the outer two zones. Analogues of Earth and Venus, on the other hand, usually contain significant amounts of material from three or four of the zones. The different composition of Earth and Venus analogues on the one hand and Mars analogues on the other is consistent with the fact that several elemental and isotopic differences are observed between these planets (see discussion in Taylor (1999)).

The degree of radial mixing is quantified and discussed further in Section 4.

4. DISCUSSION

Here we return to the questions posed in the introduction: Why do the results of earlier computer simulations differ from the terrestrial planets in the Solar System; and are the differences the result of shortcomings in the computer models, or do they indicate that our planetary system is special?

To address these questions, we need some criteria to quantify similarities and differences between systems of terrestrial planets. We can start by identifying some dynamical characteristics of the inner planets in the Solar System:

- There are four terrestrial planets.
- The largest (Earth) contains about half of the total mass.
- The planets have orbits that are widely spaced (when measured in Hill radii).
- Their orbits are almost circular.
- Their orbits are almost coplanar.
- Their spin axes are almost perpendicular to their orbital planes.
- Most of the mass is concentrated in a narrow range of heliocentric distance occupied by Venus and Earth.

To quantify these characteristics for any system of terrestrial planets, using the following statistics is suggested. Each is a dimensionless quantity, which can also be applied to satellite systems, systems of giant planets, and so forth.

- N, the number of bodies.
- The fraction of the total mass in the largest object, S_m. This statistic is unlikely to be completely independent of N, although the correlation between the two is not as strong as one might expect. For example, Saturn's satellite system contains many moons, but 96% of the total mass is contained in one object.
- An orbital spacing statistic

$$S_s = \frac{6}{N-1}\left(\frac{a_{max}-a_{min}}{a_{max}+a_{min}}\right)\left(\frac{3m_{\rm cen}}{2\bar{m}}\right)^{1/4}, \qquad (2)$$

where $\bar{m}$ is the mean mass of the planets/satellites, $m_{\rm cen}$ is the mass of the central body (e.g., the Sun), and a_{max} and a_{min} are maximum and minimum semi-major axes. This statistic is somewhat similar to the mean spacing in Hill radii. However, we can use the observation of Chambers *et al.* (1996) that the stability of a planetary system is proportional to the orbital spacing measured using a quantity, $R_{1/4}$, that varies as $m^{1/4}$ rather than the Hill radius, which varies as $m^{1/3}$. The

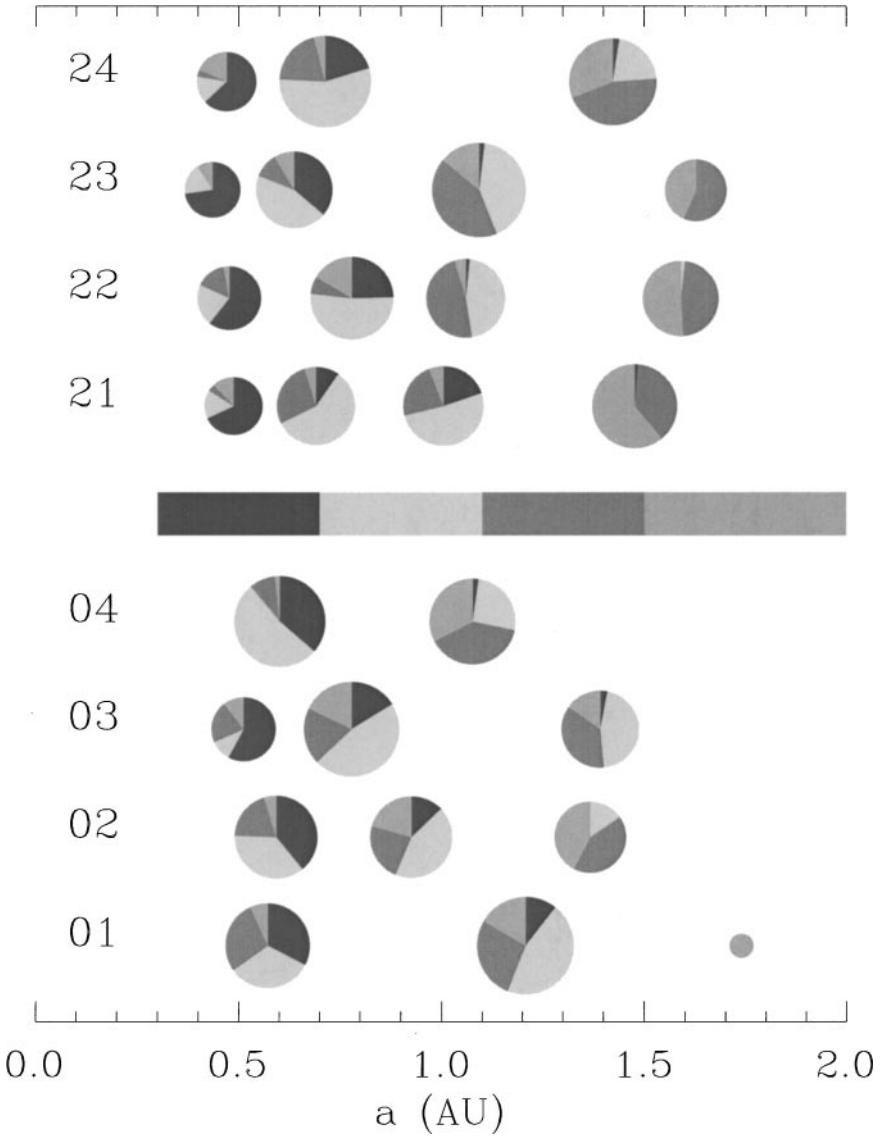

FIG. 13. Composition of the final planets in eight simulations as a function of the initial location of the embryos that comprise each object. Symbol size is proportional to the radius of each planet.

normalizing factor of 6 is chosen to make S_s similar to the mean spacing of the terrestrial planets in Hill radii.

- The normalized angular momentum deficit, S_d, defined in Eq. 1. This is chosen rather than the mass-weighted e or i since S_d generally undergoes smaller changes over time.
- An obliquity statistic

$$S_o = \left(\sum |\cos \epsilon_j| \right) \Big/ N, \tag{3}$$

where ϵ_j is the obliquity of planet j. This statistic measures the degree to which the spin axes of the planets/satellites are perpendicular to their orbital planes. Randomly orientated spin axes would make $S_o = 0.5$ on average.

- A mass-concentration statistic

$$S_c = \max \left(\frac{\Sigma m_j}{\Sigma m_j [\log_{10}(a/a_j)]^2} \right), \tag{4}$$

where m_j and a_j are the mass and semi-major axis of each planet, and S_c is given by the maximum value of the function in brackets as a function of a. This statistic measures the degree to which mass is concentrated in one part of the planetary system (e.g., in the narrow range of semi-major axes spanned by Earth and Venus in the case of the terrestrial planets). The logarithm of a is used since there is some indication that planetary spacings in the Solar System increase in proportion to heliocentric distance (the essence of the Titus–Bode law). To help understand the meaning

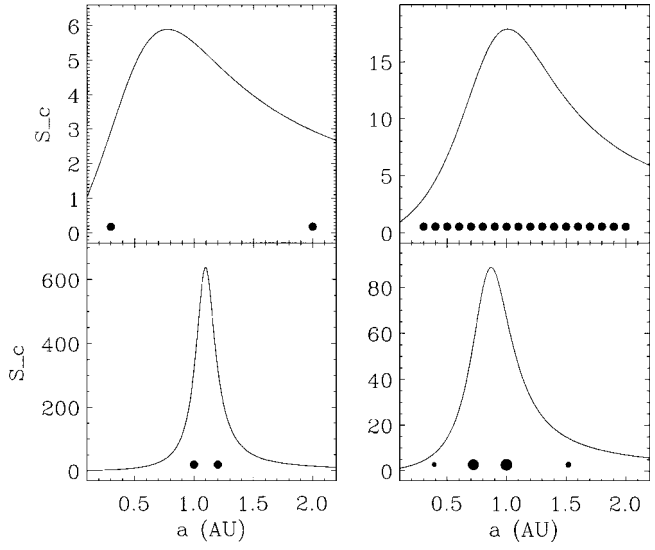

FIG. 14. Examples of the function used in the S_c statistic for four planetary systems, including the terrestrial planets (lower right). The radius of each planet is proportional to the radius of the symbol. The S_c statistic is given by the maximum value of the function.

of S_c, Fig. 14 shows some examples of the function in brackets in Eq. 4. The four panels of the figure show the function for three systems containing equal mass planets, and for the terrestrial planets of the Solar System (lower right panel). The semi-major axes of the planets in each system are shown by the circular symbols. In each panel, S_c is given by the maximum value of the curve as a function of a.

- A radial-mixing statistic

$$S_r = \left[\sum \frac{m_i |a_{init,i} - a_{fin,i}|}{a_{fin,i}} \right] \Big/ \sum m_i, \qquad (5)$$

where a_{init} and m are the initial semi-major axis and mass of each embryo that becomes incorporated into a final planet, and a_{fin} is the semi-major axis of that planet.

This statistic sums the radial migrations of each embryo that contributes toward a final planet, weighted according to the embryo's mass. The value of S_r cannot be compared directly with the terrestrial planets of the Solar System, since the source regions for the material contained in these planets is not known. However, S_r allows the degree of radial mixing to be compared between simulations.

Table I shows the values of these statistics for the planetary systems produced by the 16 simulations described in this paper. The table includes the statistics for the inner planets of the Solar System, and median values for systems produced in Paper I (note that the values of N are means rather than medians), and for another set of N-body simulations in Chambers (1998; referred to as C98 from now on), which began with 80–120 embryos and nonuniform mass distributions. Note the simulations in C98 and Paper I did not record changes in the spin states of the embryos, so it is not possible to calculate S_o in these cases. Finally, the relevant statistics for the large members of the satellites systems of Jupiter, Saturn, and Uranus are given. While it is currently unclear how these systems formed, they obey the same dynamical laws as systems of terrestrial planets. As a result, comparisons between the two should help to determine whether planetary orbits are primarily determined by processes occurring during formation, or dynamical effects subsequently.

Figure 15 shows the range of values of these statistics for the various simulations, and shows the location of the terrestrial planets within these distributions. Figure 16 indicates the degree of correlation (if any) between various pairs of statistics.

4.1. Number of Planets, Orbital Spacing, and Radial Mixing

These issues are closely related, so they are considered together. The number of final planets, N, depends on the range of their semi-major axes $a_{\max}$–$a_{\min}$, and their orbital spacing, S_s. In

TABLE I
Statistics for Final Planetary Systems

Sim	N	S_m	S_s	S_d	S_o	S_c	S_r
01	3	0.600	45.6	0.0502	0.49	38.9	0.406
02	3	0.387	36.0	0.0041	0.39	48.8	0.371
03	3	0.544	41.4	0.0102	0.86	45.1	0.420
04	2	0.545	47.2	0.0032	0.19	63.0	0.341
11	3	0.412	38.5	0.0061	0.41	40.9	0.383
12	4	0.393	37.1	0.0043	0.46	47.0	0.390
13	3	0.455	32.0	0.0045	0.33	41.7	0.337
14	2	0.722	52.1	0.0140	0.52	60.3	0.453
21	4	0.335	31.3	0.0045	0.31	37.3	0.275
22	4	0.326	33.7	0.0102	0.42	35.0	0.262
23	4	0.493	36.4	0.0048	0.73	34.8	0.263
24	3	0.471	44.7	0.0052	0.46	32.4	0.290
31	4	0.456	35.4	0.0036	0.69	36.8	0.271
32	3	0.616	42.6	0.0093	0.40	53.8	0.271
33	3	0.715	44.6	0.0060	0.33	63.8	0.341
34	3	0.616	44.9	0.0107	0.64	45.2	0.208
Paper I median	2.4	0.694	53.8	0.0228	—	39.0	
C 1998 median	3.0	0.511	42.4	0.0103	—	45.1	
01–14 median	2.9	0.500	40.0	0.0053	0.44	46.1	0.384
21–34 median	3.5	0.482	39.5	0.0056	0.44	37.1	0.273
MVEM	4	0.509	37.7	0.0018	0.96	89.9	
JSUN	4	0.715	11.6	0.0012	0.73	26.9	
Jupiter I-IV	4	0.378	16.5	4e-5	1.00	17.8	
Saturn I-VIII	8	0.955	11.4	0.0012		104.6	
Uranus I-V	5	0.386	15.6	2e-5	1.00	32.8	

Note. N is number of final planets, S_m the fraction of mass in the largest object, S_s is the orbital spacing statistic (see text), S_d is the normalized angular momentum deficit, S_o is the mean value of $|\cos\epsilon|$ where ϵ is the obliquity of each planet, S_c is the mass concentration statistic, and S_r is a radial mixing statistic (see text). "Paper I" refers to nine simulations from Model B of Paper I. "C 1998" refers to eight simulations from Chambers (1998). "MVEM" refers to the system Mercury, Venus, Earth, and Mars. "JSUN" refers to the system Jupiter, Saturn, Uranus, and Neptune.

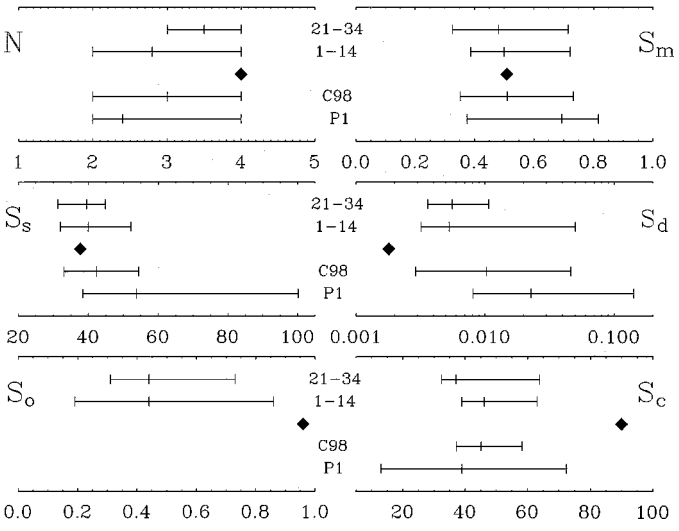

FIG. 15. Range of values of the statistics for planetary systems produced by the simulations described in this paper. The three points on each line indicate the minimum, median (mean for N) and maximum values for each set of simulations. Also shown are the statistics for simulations using Model B of Paper I (P1), and the integrations of Chambers 1998 (C98). The diamond symbols show the statistics for the terrestrial planets.

addition, if we measure orbital spacing in terms of quantities that depend on mass, such as R_H or $R_{1/4}$, the final number of planets can depend upon their masses also.

The maximum semi-major axis a that a planet in the inner Solar System can have is about 2.0 AU, which is determined by the location of the ν_6 secular resonance. The minimum value of a is less clear. The steep potential gradient close to the Sun probably prevented planets forming very much interior to the semi-major axis of the innermost planetary embryos that existed. This distance may have been determined by several factors, such as the heliocentric distance at which condensible material could exist when plantesimals and embryos were forming; the distance at which embryos would have been destroyed by collisional fragmentation (which depends on the Keplerian velocity and hence a); clearing processes associated with the young Sun; and so forth. Apparently, embryos existed at $\sim$0.4 AU in order to form Mercury, but they may also have existed closer to the Sun.

The maximum semi-major axis range constrains the maximum value of N, but not the minimum value. Terrestrial planets do not have to occupy all of the semi-major axis space available to them. For example, in the Solar System there is a wide gap between the orbit of Mars and the ν_6 resonance. As Fig. 10 shows, the outermost terrestrial planet could have formed on a stable orbit with larger a than Mars. The figure also shows a wide variety in the semi-major axis ranges of the planetary systems produced in the simulations. For example, compare simulation 12 (values of a spanning 1.4 AU) with simulation 14 (a range of 0.7 AU). These calculations began with quite similar initial conditions, yet ended very differently. Interestingly, there is quite a strong inverse correlation between N and the orbital spacing S_s in the simulations, whereas one might expect that the typical spacing would be independent of N. This suggests that the final planets retain some memory of the radial extent of the disk of embryos from which they formed; Wetherill (1994) reached a similar conclusion. In simulations with few final planets, the orbits tend to be widely spaced, occupying a greater semi-major axis range than they would do if their orbital spacing was comparable to cases with more final planets.

The orbits of the terrestrial planets are very widely spaced compared to those of the giant planets or their satellites systems (see Table I). This is true whether we measure spacing in terms of the Hill radius, R_H, which varies as $m^{1/3}$, or a quantity S_s that varies as $m^{1/4}$. The giant planets and their satellite systems may have formed in ways very different than the terrestrial planets, but each system has obeyed the same laws governing gravitational interactions since then. For example, Chambers *et al.* (1996) have shown that a system of planets with similar masses, initially moving on circular orbits, is stable for a time that depends only on the mean spacing in $R_{1/4}$. As a result, the very wide spacing of the terrestrial planets compared to other systems requires an explanation.

Laskar (1997) has made a stability analysis of the planetary system which suggests that there is no room to fit extra planets into the terrestrial region (except possibly interior to Mercury). This is because the eccentricities of the inner planets undergo large oscillations on long timescales, which would make the orbit of any intermediate planet unstable. In Laskar's model, the angular momentum deficit, S_d, of the terrestrial planets is essentially a conserved quantity, and exchange of S_d between the inner planets determines the degree of their possible radial excursions. In practice, some exchange of S_d with the outer planets occurs, but this is usually $< 50\%$ of the total value for the inner planets over the age of the Solar System; see Fig. 1 of Laskar (1997).

Hence, in Laskar's model, the S_d of Mercury, Venus, Earth, and Mars, immediately after they had accreted, determined that these would be the only terrestrial planets in the Solar System. However, this argument does not explain why the Solar System has four terrestrial planets. To see this, imagine that the semi-major axes of the inner planets were rearranged, placing them slightly closer together, and making use of the space interior to Mercury and exterior to Mars. In addition, suppose that the $\sim 2 M_\odot$ of mass contained in the inner planets was redistributed so that the planets either had a larger or smaller range of masses than today. Using some combination of these processes, it seems likely that systems of five or even six terrestrial planets could exist, with stable orbits, and with the same value of S_d as the inner planets of the Solar System. Conversely, it is certainly true that fewer than four inner planets could exist, with the same total mass and angular momentum deficit as the terrestrial planets. So, while the model of Laskar (1997) makes an important contribution to our understanding of the configuration of the inner planets, it is clearly not the whole story.

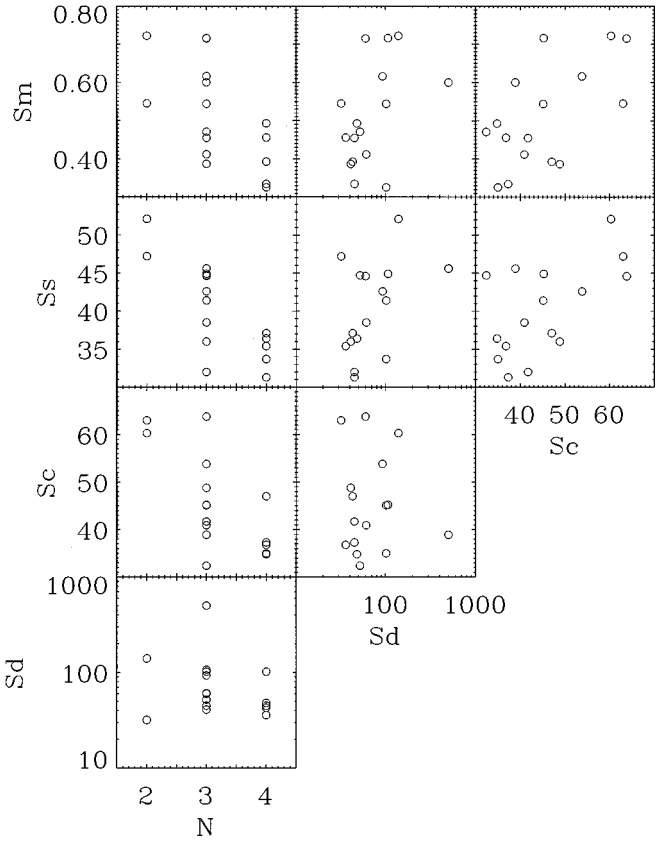

FIG. 16. Correlations between some of the S statistics for simulations 01–34.

There are several reasons for thinking that the number of terrestrial planets in the Solar System is not determined by their current angular momentum deficit. First, the normalized angular momentum deficit S_d for the giant planets is similar to that for the terrestrial planets (i.e., their eccentricities and inclinations are comparable), but the giant planets have a much smaller spacing S_s. Second, in the simulations presented here, there is no correlation between S_d, and the orbital spacing S_s, or between S_d and N (see Fig. 16). For example, simulation 22 ended with four planets having S_d five times larger than that of the terrestrial planets, yet the planets in the simulation actually had a smaller separation. (Note, however, that this system was not integrated for the age of the Solar System—it may not be stable for this length of time.) Third, systems with large S_d, such as the Upsilon Andromedae planetary system ($S_d = 0.038$ assuming coplanar orbits) can have a much smaller spacing ($S_s = 14.4$) than the terrestrial planets, even though the Ups. And. system is stable for > 1 billion years (Rivera and Lissauer 2000).

Therefore, the number and spacing of the terrestrial planets requires another explanation. In particular, we need to address the question of why the inner planets are spaced so much more widely than the giant planets of the Solar System. One idea is that the giant planets can have smaller spacings because they are essentially an autonomous system, while the inner planets are perturbed by the outer planets. However, this argument is unconvincing, since as Laskar (1997) has pointed out, the outer and inner planets trade only modest amounts of energy and angular momentum. In particular, the largest angular momentum deficit achieved by the inner planets in Laskar's 25 billion year calculation is still less than the typical value for the systems with $N = 4$ described in this paper.

A more likely explanation for the large spacings of the terrestrial planets is that they are the result of processes occurring during their formation. Re-examining Figs. 1–4 and Fig. 9, there is a strong suggestion that the spacing of the final planets is determined by the amplitude of their radial excursions during their accretion (c.f. Chambers 1997). Radial excursions are caused by nonzero eccentricity e, oscillations in e because of secular interactions, and changes in semi-major axis resulting from close encounters. The giant planets play an important role in these processes (see Ito and Tanikawa 1999), in particular by exciting the orbits of bodies near the ν_6 resonance. Some of these objects then go on to interact with bodies closer to the Sun. The combined effect of these processes generally causes protoplanets to have larger radial excursions during their formation than after accretion is complete. Once accretion is complete, planets tend to undergo only very small changes in a, and in a number of cases the maximum value of a planet's eccentricity is smaller after accretion than during accretion (e.g., simulations 03 and 13 in Fig. 9). This may also have been the case for the terrestrial planets of the Solar System.

Figure 17 demonstrates this argument more clearly. The figure shows the perihelion and aphelion distances for each object destined to become a final planet in the simulations depicted in Figs. 1–4. Also shown is the perihelion and aphelion distance of the most massive body in each simulation that did not survive. In general, the radial excurisons of each protoplanet span sufficiently large parts of the inner Solar System that there is no room for other bodies to exist on stable orbits in between them. Each of the nonsurviving bodies is forced onto an orbit that crosses one of the others, leading to a collision.

None of the simulations in this paper, or those of Paper I or C98, in which the giant planets were present, ended with more than four terrestrial planets. Conversely, several of the simulations of Wetherill (1986), Cox and Lewis (1980), Lecar and Aarseth (1986), Agnor *et al.* (1999), for example, which neglected giant-planet perturbations, did end with more than four inner planets (note that some of these calculations also neglected some long-range forces between planetary embryos). This is consistent with the idea that perturbations from the giant planets, while the inner planets were still accreting, helped to determine how many terrestrial planets would form. Future simulations using different giant-planet characteristics may shed some light on this issue.

The N-body integrations of Paper I almost always ended with fewer than four planets—typically only two, and in extreme cases, only one. The simulations of C98, which began with more

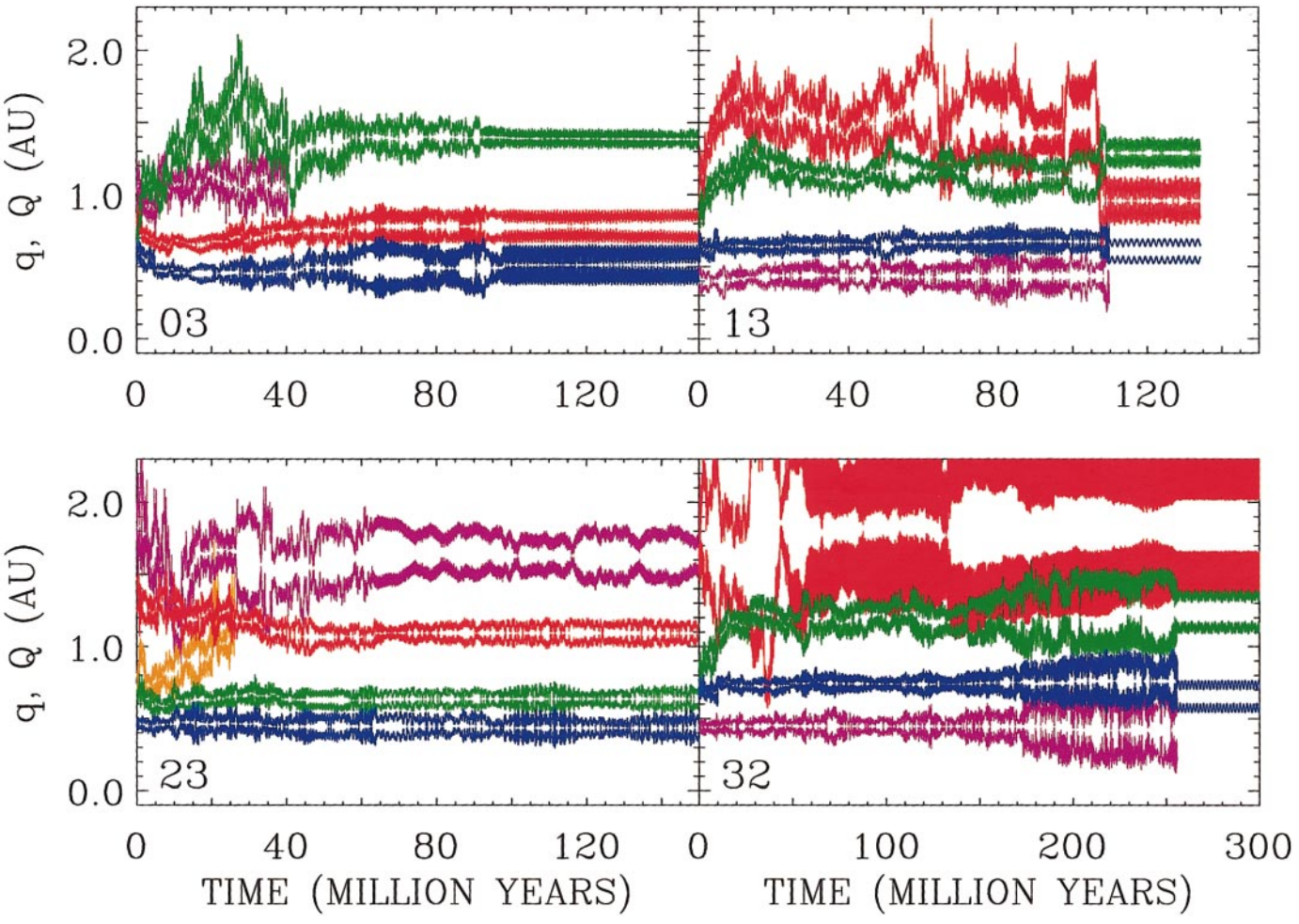

FIG. 17. Perihelion and aphelion distances for objects destined to become final planets, plus the most massive non-surviving object, in the simulations of Figs. 1–4.

embryos, often produced systems of three planets, and occasionally four. In this paper, which started with still more embryos, half of simulations 21–34 ended with four planets.

The results of these N-body integrations suggest that starting with more embryos increases the final number of terrestrial planets. However, a second factor seems to be at least as important: the initial mass distribution. The bimodal mass distribution of simulations 21–34 yielded more planets than the approximately uniform mass distribution of simulations 1–14. In addition, the simulations of C98 ended with slightly more planets on average than simulations 1–14 of this paper, despite starting with fewer embryos. In C98, the embryos masses, m, were drawn from a probability distribution function $f(m)\,dm \sim m^{-2}dm$, so that there were many small embryos and a few large ones.

Hence, a protoplanetary disk containing embryos with a wide range of masses is likely to yield more terrestrial planets than a uniform mass distribution. The reason for this seems to be that massive embryos are less mobile and more isolated from one another when a large population of smaller bodies is present. Dynamical friction tends to keep e small for the largest bodies, and close encounters between large and small objects induce little radial migration in the former. As a result, the radial excursions of the largest bodies are somewhat smaller than they would be in the absence of small bodies (which was basically the situation in Paper I). This increases the likelihood that four large bodies will form on widely separated orbits and remain there. This is consistent with the observation that the material in the final planets in simulations 21–34 was less well mixed than that in the planets in the uniform-mass integrations. The radial mixing statistics, S_r, for simulations 21–34 are significantly smaller than those for simulations 1–14: 0.27 ± 0.04 compared to 0.39 ± 0.04.

Finally, luck plays a big role in determining the outcome of some of the simulations. For example, in simulation 13, a system of four planets had formed after 100 million years, which bore some resemblence to the terrestrial planets. However, the system was unstable on a timescale of several tens of millions

of years, and further accretion took place subsequently. Something similar may have happened in many extrasolar systems, and the terrestrial planets in the Solar System could be a lucky exception.

4.2. Mass of Largest Planet

The Earth contains slightly more than half of the total mass contained in the terrestrial planets. As noted earlier, the fraction of mass contained in the largest body in a system, S_m, is not necessarily a function of the number of objects in the system. For example, Titan contains 96% of the total mass in the eight large Saturnian satellites. By contrast, Ganymede contains less than 40% of the mass contained in the four Galilean satellites of Jupiter, even though this system has fewer members.

Having said this, there is an anticorrelation between N and S_m for the simulations in Paper I, those of C98 and those presented here (see Fig. 16). In Paper I, the majority of the surviving mass at the end of each integration was usually contained in a single body because in many cases only two final planets formed. The integrations of C98 and those presented here typically had smaller values of S_m, while N was more likely to be 3 or 4. The newer simulations produced similar ranges in S_m, with medians close to the value for the terrestrial planets in each case. In C98 and simulations 1–34, the largest final planet contained 1/3 to 2/3 of the remaining mass, and this range was independent of the initial mass distribution. The good agreement between observed and calculated values of S_m can be considered a success of the model and simulations described here.

In agreement with Wetherill (1992, 1996), the largest planets seen in Fig. 11 tended to form at heliocentric distances comparable to Earth and Venus. In contrast, in Paper I, large planets also formed at smaller distances. The late stages of the simulations in Paper I typically consisted of a handful of large bodies, containing most of the remaining mass, moving on crossing orbits. These objects scattered off one another and/or accreted to produce a final system of planets. Bodies in the inner part of the disk had higher collision probabilities (because of the smaller radii of their orbits), and tended to form large final planets. Bodies in the outer part of the disk had lower collision probabilities and tended to remain smaller by comparison. In the simulations presented here, the largest bodies remained more isolated from one another than in the earlier calculations, because of dynamical friction with a population of smaller bodies. This tended to keep the largest bodies rather localized, and as a result, large planets formed in the middle region of the disk where the surface density was highest, and where they had access to planetesimals from both the inner and outer parts of the disk.

4.3. Normalized Angular Momentum Deficit

The orbits of the terrestrial planets are approximately circular and lie close to the invariable plane of the planetary system. However, their e and i are not exactly zero, so the terrestrial planet system has a (normalized) angular momentum deficit. This is currently about 0.0014, and slightly larger (0.0018) when averaged over million-year timespans.

The planetary systems described in this paper all have larger values of S_d than the terrestrial planets, typically 2 to 3 times greater and occasionally much more. The values of S_d are generally lower than those for the simulations in Paper I, and the median value of S_d is significantly lower than for the integrations in Paper I and C98. This is reflected in the typically lower eccentricities of the final planets in the upper panel of Fig. 12 compared to the lower panel. In addition, the planets produced in the new simulations generally have lower eccentricities than the planets produced by Agnor *et al.* (1999). These authors used an initial number of embryos similar to the integrations in Paper I. These differences can be attributed to the greater effects of dynamical friction in the new simulations because of the larger initial number of planetary embryos, N_0, which allows a wider spectrum of embryos masses to develop. This suggests that the high final eccentricities found in the earlier N-body simulations, and to a lesser extent those presented here, are an artifact caused by starting with too few embryos. If this is true, simulations beginning with several hundred embryos could produce planetary systems with angular momentum deficits comparable to the terrestrial planets.

The initial mass distribution may also make a difference to the S_d of the final system. Comparing the results of simulations 01–14 with 21–34, there is some hint that systems with large S_d are less likely to occur when the embryos have a bimodal mass distribution. However, the median values of S_d are similar for the two batches of integrations, so this result may be an artifact resulting from the small number of simulations.

Incidentally, the e and i situation looks rather better if we compare the mass-weighted eccentricities, $\bar{e}$, and inclinations, $\bar{i}$, of the simulated systems with the terrestrial planets (Chambers and Lissauer 2000). In this case, the range of values for simulations 01–34 ($0.036 < \bar{e} < 0.27$ and $1.5 < \bar{i} < 6.6^\circ$) extend all the way down to the values for the terrestrial planets ($\bar{e} = 0.04$ and $\bar{i} = 2^\circ$).

4.4. Obliquities

The planets produced in simulations 01–34 have randomly orientated spin axes, leading to S_o values clustered around 0.5. This result confirms the earlier findings of Agnor *et al.* (1999) that primordial spins are randomly determined by one or two giant impacts during accretion. Conversely, the terrestrial planets all have spin axes that are roughly perpendicular to their orbital planes, which gives the system an obliquity statistic, S_o close to unity. However, the current spin axes of the terrestrial planets are unlikely to be primordial (see Lissauer and Kary 1991, Laskar and Robutel 1993), so this does not imply that giant impacts, of the kind seen in the simulations, did not occur.

4.5. Planetary Masses and Mass Concentration

The simulations in this paper produced a number of planets with semi-major axes comparable to Mercury or Mars. However, these bodies typically have masses in the range 0.2–0.6$M_\oplus$, compared to 0.06 and 0.1 for Mercury and Mars, respectively. The mass resolution of the simulations was sufficient that three cases ended with planets having roughly lunar mass. However, all these bodies have $a > 1.7$ AU, lying just inside the asteroid belt. In contrast, bodies with masses in the range 0.02–0.2$M_\oplus$ are absent. This is particularly puzzling for simulations 21–34 with bimodal initial mass distributions. In these cases, the large embryos began with masses comparable to Mars, and could have made excellent Mars analogues had they survived unaltered. This did not happen. Instead, these embryos accreted or were themselves accreted to form larger planets. The only low-mass planet formed in simulations 21–34 was an unaltered small embryo with sublunar mass.

Ninety percent of the mass in the inner Solar System is concentrated in bodies which orbit in a narrow range of heliocentric distance between 0.7 and 1.0 AU. However, models for the Sun's protoplanetary nebula (e.g., Bell *et al.* 1997) typically predict a relatively smooth distribution of mass with distance from the Sun at the time that planetesimals formed. Clearly the mass distribution became uneven over time as accretion led to larger bodies, but this does not explain why Earth and Venus accreted so much more material than Mercury and Mars, or why these two large planets have orbits so close to one another. This problem has been apparent for some time (it can be seen in the results of Wetherill 1992), but it has received less attention than the eccentricity/inclination and obliquity problems described above.

The mass concentration statistic, S_c, defined earlier, gives a measure of this problem. The terrestrial planets have $S_c = 90$, which is larger than that for any of the systems produced in this paper or in Paper I. It is also much higher than the values of S_c for the giant planets, and the satellite systems of Jupiter and Uranus (see Table I). Only the Saturnian satellite system, in which ∼96% of the mass is concentrated in Titan, has a larger value of S_c.

Unlike the problem of large e and i, this problem shows no sign of going away as the initial number of embryos is increased or different initial mass distributions are adopted. The simulations of Paper I, C98, and those presented here produced systems with similar median values of S_c, and a roughly comparable range of values. Even the extreme cases lie far from the value of S_c for the terrestrial planets. The simulations of Agnor *et al.* (1999) and Wetherill (1996) also typically produced Mars and Mercury analogues with masses of 0.2–0.6$M_\oplus$, while bodies with lower masses were uncommon. This suggests that these systems too would have smaller values of S_c than the terrestrial planets. This common outcome occurred despite the fact that these simulations used different initial conditions from the ones presented here, and the simulations of Wetherill used a completely independent technique.

There are two ways to explain the high concentration of mass in Venus and Earth: Either the mass of solid bodies in the protoplanetary disk was lower in the regions now occupied by Mars and Mercury, or mass was preferentially lost from these regions during the accretion of the planets. If the first explanation is correct, this argues for a surface density profile of solids in the nebula that was distinctly nonmonotonic. Simulations of the formation of Jupiter via core accretion suggest that the surface density of solid material at 5 AU was $\sim 10\,\mathrm{g\,cm^{-2}}$ (Pollack *et al.* 1996), comparable to the value at 1 AU needed to form the Earth. The mass depletion in the Mars and Mercury regions must have been severe—the simulations described here were deliberately started with a surface density profile that peaked sharply near Venus and Earth, and yet the mass contained in the final planets was quite spread out.

Alternatively, some process may have preferentially removed solid mass from the Mars and Mercury regions. Collisional fragmentation and the effects of resonances with the giant planets are two possibilities. In the inner part of the disk, currently occupied by Mercury, a substantial amount of mass may have been lost by catastrophic collisions between planetary embryos. Orbital velocities are high this close to the Sun, which increases the typical velocity of impacts striking embryos, and this increases the amount of material which escapes in fragments. The high density of Mercury suggests that it may be the surviving core of a larger differentiated body disrupted in a high-velocity impact (Wetherill 1988).

The simulations in this paper began with low-surface densities in the inner part of the disk in order to model the effects of this mass loss process, but the integrations failed to produce Mercury sized planets close to the Sun. This suggests that the effects of collisional fragmentation are larger than allowed for here. A second possibility is that the disk of embryos did not extend to small enough semi-major axes. Some low-mass Mercury analogues did form in the simulations, but these formed close to analogues of Venus and were subsequently accreted by this planet.

Collisional fragmentation alone seems unlikely to explain the low mass of Mars. Orbital velocities in this region are lower than those near Earth and Venus, although Mars lies closer to the ν_6 secular resonance, which excites orbital eccentricities to large values (see Figs. 1–4). Some objects moving on highly eccentric orbits would have crossed the orbit of the early Mars, possibly leading to high-velocity erosional impacts. However, extrapolating the results of recent computer simulations of impacts (Melosh and Ryan 1997, Benz and Asphaug 1999) suggests that high-velocity impacts onto a body the size of Mars are unlikely to remove much material in escaping fragments. For example, using the impact energy scaling relation of Melosh and Ryan (1997), Agnor *et al.* (1999) estimate that only a few percent of material escapes during collisions typical of those in late-stage terrestrial planet formation. The author is currently making a new set of N-body simulations, including a model for fragmentation, to see if collisional erosion effects the masses of Mars and Mercury analogues.

Alternatively, mass could have been removed from the Mars region by the same mechanism that cleared most of the primordial solid mass from the main asteroid belt. There are several hypotheses to explain mass loss from the belt (see for example, Morbidelli *et al.* 2000 and Chambers and Wetherill 2001), but all rely on the presence of unstable resonances with the giant planets. These resonances do not extend inside 2.1 AU at present, although they may have existed closer to the Sun at the time at which the terrestrial planets were forming (e.g., Nagasawa *et al.* 2000).

4.6. Summary

The simulations presented in this paper typically produced systems of three or four planets (the latter in 50% of cases using bimodal mass distributions). The largest planet in each case contained 1/3 to 2/3 of the final mass, and the planets had very large orbital spacings. These characteristics are all similar to those of the terrestrial planets, and the model described here can be considered successful in these respects.

The planets produced by the integrations usually had orbits with higher eccentricities, e, and inclinations, i, than Earth and Venus. However, the situation is a substantial improvement over the results of Paper I. In addition, the values of e and i are becoming smaller, as the initial number of embryos is increased, suggesting that this discrepancy between model and observation may disappear in simulations starting with more embryos (possibly as few as several hundred).

The obliquities of the simulation planets are randomly distributed, in marked contrast to the terrestrial planets, whose current spin axes are more or less perpendicular to their orbital planes. However, the spin axes of the terrestrial planets are not primordial, so this does not necessarily indicate a problem with the models used here.

Finally, the high concentration of mass in the region occupied by Venus and Earth is not reproduced in any of the simulations, and this discrepancy shows no sign of disappearing as a result of using different initial conditions. This represents perhaps the most important outstanding problem for theories of the final stage of terrestrial planet formation.

ACKNOWLEDGMENTS

The author thanks Lindsey Bruesch, David Catling, Monika Kress, Jack Lissauer, George Wetherill, Kevin Zahnle, and others for discussions and ideas during the preparation of this paper. Many thanks also to Martin Murphy and Eugenio Rivera for a great deal of computer help and support. This work was supported by DENI, NRC, PPARC, and Starlink. Apologies to Slartibartfast—I'll do better next time.

REFERENCES

Agnor, C. B., R. M. Canup, and H. F. Levison 1999. On the character and consequences of large impacts in the late stage of terrestrial planet formation. *Icarus* **142**, 219–237.

Alexander, S. G., and C. B. Agnor 1998. *Icarus* **132**, 113–124.

Beaugé, C., and S. J. Aarseth 1990. N-body simulations of planetary formation. *Mon. Not. R. Astron. Soc.* **245**, 30–39.

Bell, K. R., P. M. Cassen, H. H. Klahr, and Th. Henning 1997. The structure and appearance of protostellar accretion disks: Limits on disk flaring. *Astrophys. J.* **486**, 372–387.

Benz, W., and E. Asphaug 1999. Catastrophic disruptions revisited. *Icarus* **142**, 5–20.

Chambers, J. E. 1997. A possible explanation for the spacing of the terrestrial planets. In *Proceedings of the 9th Rencontres de Blois: Planetary Systems: The Long-term view,* in press.

Chambers, J. E. 1998. N-Body Simulations of Planet Formation: Varying the Initial Number of Planetary Embryos. *Earth, Moon, Planets* **81**, 3–6. (C98)

Chambers, J. E. 1999. A hybrid symplectic integrator that permits close encounters between massive bodies. *Mon. Not. R. Astron. Soc.* **304**, 793–799.

Chambers, J. E., and F. Migliorini 1997. Mercury—A New software package for orbital integrations. *BAAS* **29**, 1024.

Chambers, J. E., and G. W. Wetherill 1998. Making the terrestrial planets: N-Body integrations of planetary embryos in three dimensions. *Icarus* **136**, 304–327. (Paper I)

Chambers, J. E., and J. J. Lissauer 2000. The good, the bad and the ugly: assessing the results of planetary accretion simulations. Abstract presented at the 2000 meeting of the DDA, Yosemite, CA.

Chambers, J. E., and G. W. Wetherill 2001. Planets in the asteroid belt. *Meteoritics Plan. Sci.* **36**, 381–399.

Chambers, J. E., G. W. Wetherill, and A. P. Boss 1996. The stability of multi-planet systems. *Icarus* **119**, 261–268.

Cox, L. P., and J. S. Lewis 1980. Numerical simulation of the final stages of terrestrial planet formation. *Icarus* **44**, 706–721.

Gladman, B. J., F. Migliorini, A. Morbidelli, V. Zappala, P. Michel, A. Cellino, C. Froeschle, H. F. Levison, M. Bailey, and M. Duncan 1997. Dynamical lifetimes of objects injected into asteroid belt resonance. *Science* **277**, 197–201.

Ito, T., and K. Tanikawa 1999. Stability and instability of the terrestrial protoplanet system and their possible roles in the final stage of planet formation. *Icarus* **139**, 336–349.

Kokubo, E., and S. Ida 1998. Oligarchic growth of protoplanets. *Icarus* **131**, 171–178.

Kokubo, E., and S. Ida 2000. Formation of protoplanets from planetesimals in the solar nebula. *Icarus* **143**, 15–27.

Laskar, J. 1997. Large scale chaos and the spacing of the inner planets. *Astron. Astrophys.* **317**, L75–L78.

Laskar, J., and P. Robutel 1993. The chaotic obliquity of the planets. *Nature* **361**, 608–612.

Lecar, M., and S. J. Aarseth 1986. A numerical simulation of the formation of the terrestrial planets. *Astrophys J.* **305**, 564–579.

Lissauer, J. J. 1993. Planet formation. *Ann. Rev. Astron. Astrophys.* **31**, 129–174.

Lissauer, J. J., and D. M. Kary 1991. The origin of the systematic component of planetary rotation. I—Planet on a circular orbit. *Icarus* **94**, 126–159.

Melosh, H. J., and E. V. Ryan 1997. Asteroids: Shattered but not dispersed. *Icarus* **129**, 562–564.

Morbidelli, A., J. Chambers, J. I. Lunine, J. M. Petit, F. Robert, G. R. Valsecchi, and K. E. Cyr 2000. Source regions and timescales for the delivery of water to the Earth. *Meteoritics Plan. Sci.* **35**, 1309–1320.

Nagasawa, M., H. Tanaka and S. Ida 2000. Orbital evolution of asteroids during depletion of the solar nebula. *Astron. J.* **119**, 1480–1497.

Pollack, J. B., O. Hubickyj, P. Bodenheimer, J. J. Lissauer, M. Podolak and Y. Greenzweig 1996. Formation of the giant planets by concurrent accretion of solids and gas. *Icarus* **124**, 62–85.

Rivera, E. J., and J. J. Lissauer 2000. Stability analysis of the planetary system orbiting υ andromedae. *Astrophys. J.* **530**, 454–463.

Safronov, V. 1969. Evolution of the Protoplanetary Cloud and Formation of the Earth and Planets. Moscow: Nauka. English translation, NASA TTF-677, 1972.

Taylor, S. R. 1999. Leonard award address—On the difficulties of making earth-Like planets. *Meteoritics Plan. Sci.* **34**, 317–330.

Weidenschilling, S. J. 1977. The distribution of mass in the planetary system and solar nebula. *Icarus* **51**, 153–158.

Weidenschilling, S. J., D. Spaute, D. R. Davis, F. Marzari, and K. Ohtsuki 1997. Accretional evolution of a planetesimal swarm. 2. The terrestrial zone. *Icarus* **128**, 429–455.

Wetherill, G. W. 1986. Accumulation of the Terrestrial Planets and Implications Concerning Lunar Origin. In *Origin of the Moon; Proceedings of the Conference*, Lunar Planet. Inst., Houston, pp. 519–550.

Wetherill, G. W. 1988. Accumulation of mercury from planetesimals. In *Mercury*, pp. 670–691. Univ. of Arizona Press, Tucson.

Wetherill, G. W. 1992. An alternative model for the formation of the asteroids. *Icarus* **100**, 307–325.

Wetherill, G. W. 1994. Provenance of the terrestrial planets. *Geochim. Cosmochim. Acta* **58**, 4513–4520.

Wetherill, G. W. 1996. The formation and habitability of extra-solar planets. *Icarus* **119**, 219–238.

Wetherill, G. W., and G. R. Stewart 1989. Accumulation of a swarm of small planetesimals. *Icarus* **77**, 330–357.

Wetherill, G. W., and G. R. Stewart 1993. Formation of planetary embryos: Effects of fragmentation, low relative velocity, and independent variation of eccentricity and inclination. *Icarus* **106**, 190–209.